









Cite this: *Nanoscale*, 2017, 9, 6558

# Ultrafast transient optical loss dynamics in exciton–plasmon nano-assemblies†

Mohamed ElKabbash, \*‡<sup>a</sup> Alireza R. Rashed, ‡<sup>a,b</sup> Betul Kucukoz, <sup>c</sup>  
 Quang Nguyen, <sup>a</sup> Ahmet Karatay, <sup>c</sup> Gul Yaglioglu, <sup>c</sup> Ekmel Ozbay, <sup>b</sup>  
 Humeyra Caglayan ‡<sup>b</sup> and Giuseppe Strangi \*‡<sup>a,d</sup>

We study the exciton–plasmon dynamics that lead to optical loss mitigation *via* ultrafast transient absorption spectroscopy (UTAS) on hybrid aggregates of core–shell quantum dots (QDs) and Au nanoparticles (NPs). We highlight that generating hot electrons in plasmonic NPs contributes to the transient differential absorption spectrum under optical excitation. The results suggest modifying the method of analyzing the transient absorption spectra of loss mitigated systems. Additionally, we investigate the effect of Electron Oscillation frequency-Phonon Resonance Detuning (EOPRD) on loss mitigation efficiency. Moreover, power dependent UTAS reveal a frequency pulling like effect in the transient bleach maximum towards the gain emission. We show that the appropriate choice of the pump wavelength and by changing the pump power we can conclusively prove the existence of loss mitigation using UTAS. Finally, we study the transient kinetics of hybrid gain–plasmon systems and report interesting hybrid transient kinetics.

Received 2nd March 2017,

Accepted 31st March 2017

DOI: 10.1039/c7nr01512g

rsc.li/nanoscale

## 1 Introduction

Surface plasmons (SPs) are quasi-particles that result from coupling an electromagnetic (EM) field to free electrons that collectively oscillate at an interface where the real part of the dielectric function changes signs. The field of plasmonics utilizes SPs for many applications in different technological areas.<sup>1–4</sup> Except for low efficiency applications that are not affected much by losses<sup>5–7</sup> such as surface enhanced Raman spectroscopy (SERS), perfect light absorption and photo-thermal cancer therapy, the strong absorption and optical losses in the available plasmonic materials are the main obstacles for their promising applications.

EM field confinement is the major advantage of plasmonics. The ability to confine the EM field beyond the diffraction limit requires the existence of free electrons. In general the EM field achieves self-sustaining oscillations by transferring the conserved energy between its electric and magnetic components. However, this self-sustaining oscillation is not poss-

ible beyond the diffraction limit, *i.e.* below  $\lambda/2n$ , because in a deeply sub-wavelength regime the electric (magnetic) field will not get a chance to fully develop its magnetic (electric) counterpart to conserve the total energy.<sup>8</sup> On the other hand, by storing some of the EM energy in the kinetic energy of resonant free electrons in metals (*i.e.* SPs), sub-wavelength self-sustained oscillation will be possible. In that sense, one can think of a plasmonic NP as a leaky cavity. The motion of such free electrons is inevitably damped due to electron scattering events creating a causal link between the excitation of free electrons (SPs) and loss of EM energy.

Localized surface plasmons (LSPs) are excited in nanoparticles (NPs) with free electrons (*e.g.* metals or doped semiconductors) that are dimensionally comparable or smaller than the wavelength of the resonant electromagnetic field. Absorption of the EM field results from electron scattering events which are mainly electron–phonon scattering, electron–surface scattering and inter-band transitions.<sup>8,9</sup> These loss channels broaden the plasmon resonance spectrally creating what is called a plasmon band. For instance, the plasmon band of Ag is narrower and sharper than that of Au because the electronic inter-band transition in Au spectrally coincides with the SP resonance, thus adding an extra loss channel.

One possible scheme to deal with losses in plasmonics while maintaining the EM sub-wavelength confinement is to introduce gain in the dielectric surrounding of the plasmonic NPs such that the gain emission spectrally overlaps with the plasmon band.<sup>10–12</sup> The gain provides an energy source that compensates the optical losses and thus maintains self-sus-

<sup>a</sup>Department of Physics, Case Western Reserve University, 2076 Adelbert Road, Cleveland, Ohio, 44106-7079, USA. E-mail: gxs284@case.edu, mke23@case.edu

<sup>b</sup>Nanotechnology Research Center, Bilkent University, 06800 Ankara, Turkey

<sup>c</sup>Department of Engineering Physics, Faculty of Engineering, Ankara University, 06100 Ankara, Turkey

<sup>d</sup>Department of Physics and CNR - Nanotec, University of Calabria, 87036 Rende, Italy

†Electronic supplementary information (ESI) available. See DOI: 10.1039/c7nr01512g

‡These authors contributed equally to this work.

taining oscillation of the EM field while keeping the sub-wavelength field confinement in the vicinity of the NP. This energy transfer takes place through dipole–dipole non-radiative resonant energy transfer between the excitonic element (donor) and plasmonic NPs (acceptor). The resonance condition is satisfied when the donor emission spectrally overlaps with the SP resonance of the acceptor. The energy transfer process is irreversible and thus the gain is weakly coupled to the plasmonic NP. This effect has been experimentally investigated by using reflection and transmission pump–probe spectroscopies complemented by fluorescence time-resolved spectroscopy.<sup>13–16</sup> In addition, transient absorption spectroscopy (TAS) has been employed to verify the existence of loss mitigation effects.<sup>17–19</sup>

However, a systematic and detailed study utilizing pump–probe transient absorption spectroscopy on hybrid gain–plasmon systems has not been performed to date. In addition, previous theoretical<sup>15,16</sup> and experimental<sup>14,17</sup> works have neglected the effect of the pump beam on the NP optical properties. This is a significant issue since it can result in experimental artifacts for the optical characterization of plasmonic materials.

In this work, we study the transient absorption of resonant gain–plasmon aggregates as hybrid nano-assemblies and their ultrafast transient kinetics. We perform detailed pump–probe transient absorption spectroscopy experiments to investigate the loss mitigation process of aggregated Au NPs in the close vicinity of core–shell QDs. We show that the enhanced transmission could be due to other effects occurring in the material during optical pumping and probing processes and that these effects can be misinterpreted as loss mitigation. Furthermore, we highlight the transient nature of the plasmon band quality factor and the effect of Electron Oscillation frequency-Phonon Resonance Detuning (EOPRD) on loss mitigation efficiency. Additionally, we show that the loss mitigation of NP aggregates occurs for the subset of plasmon resonances that overlap with the gain emission and that the loss mitigation efficiency is wavelength dependent. Such wavelength dependence is translated in the dependence of the loss mitigation maximum wavelength on pump power, which has been predicted theoretically,<sup>15</sup> and in the effect of EOPRD on loss mitigation at different wavelengths. Finally, we study the transient kinetics of loss mitigated systems and the effect of NP-gain relative concentrations on the dynamics of loss mitigation. In addition to understanding the dynamics of optical loss mitigation in resonant gain–plasmon nano-assemblies, we provide new insights regarding engineering hybrid gain–plasmon systems to unlock potential applications of plasmonic nanostructures.

The measurements are carried out on three systems: (a) a polydimethylsiloxane (PDMS) host doped with aggregates of core–shell CdSe@ZnS QDs; this is the Gain System (GS), (b) a PDMS host doped with aggregates of 11 nm Au NPs, in two different concentrations; lower concentration (**AuL**) of  $1 \times 10^{-6}$  M and higher concentration (**AuH**) of  $3 \times 10^{-6}$  M, and (c) a PDMS host containing a mixture of QDs and Au NPs with the same concentration of QDs in GS and the same concentration

of Au NPs of **AuL** (for **GS\_AuL**) and **AuH** (for **GS\_AuH**). Fig. 1(a) shows a scheme of the three systems.

## 2 Results and discussion

### 2.1 Samples characterization

The extinction and emission curves of GS as well as the extinction of both **AuL** and **GS\_AuL** are presented in Fig. 1(b) and (c), respectively. According to Fig. 1(c), the broad extinction peak of **AuL** is centered at roughly 610 nm. The broadening of the plasmon band is due to NP aggregation within the polymer.<sup>20</sup>

Furthermore, **GS\_AuL** extinction reflects the extinction of aggregates of both QDs and NPs exhibiting a peak at  $\approx 553$  nm. This is not the true plasmon resonance extinction peak due to the influence of the QDs' extinction. Our analysis (see ESI section 1†) shows that the plasmon extinction peak wavelength of **GS\_AuL** is  $\approx 590$  nm. The emission of the embedded QDs is roughly the same for GS and **GS\_AuL**. The emission maximum of QDs is at  $\approx 570$  nm overlapping with the plasmon band of **GS\_AuL** and thus satisfying the loss mitigation non-radiative resonant energy transfer condition.

### 2.2 Ultrafast transient absorption spectroscopy measurements (UTAS)

After exciting the sample by an ultrafast pump pulse, a temporally delayed probe pulse is used to extract the pump-induced absorbance change of the sample. The experimental setup details are provided in the Experimental section. By measuring the wavelength-dependent intensity of the delayed probe spectra in the presence ( $I_{\lambda,t}$ ) and the absence ( $I_{\lambda,0}$ ) of the pump pulses, the transient absorption signal  $S(\lambda,t)$  is calculated based on the following equation:

$$S(\lambda,t) = \frac{\Delta T}{T_0} = -(I_{\lambda,t} - I_{\lambda,0})/I_{\lambda,0} \quad (1)$$

Note that according to our sign convention, a positive sign of the pump–probe differential transmission ( $\Delta T/T_0$ ) corresponds to a decrease in transmission (transient absorption), whereas a negative sign of  $\Delta T/T_0$  corresponds to an increase in transmission (transient bleach).

The measurements were performed by using 400 nm and 800 nm excitation wavelengths in order to independently probe the effect of gain excitation and energy transfer processes on the transient absorption signal. In addition, the delay between the pump and probe was varied to observe the modification of the transient absorption signal over time and to examine the transient decay kinetics of all the systems.

Transient absorption (TA) measurements for the GS sample (see Fig. 2(a)) are performed using a 400 nm wavelength pump at 1  $\mu$ J for 650 fs, 33 ps, and 1 ns delay times. The maximum bleach wavelength is  $\approx 550$  nm which is close to the local absorption maxima shown in Fig. 1(b). As we increase the delay time the bleach initially increases in magnitude, reaching its maximum at 650 fs, and then it starts to decrease. The

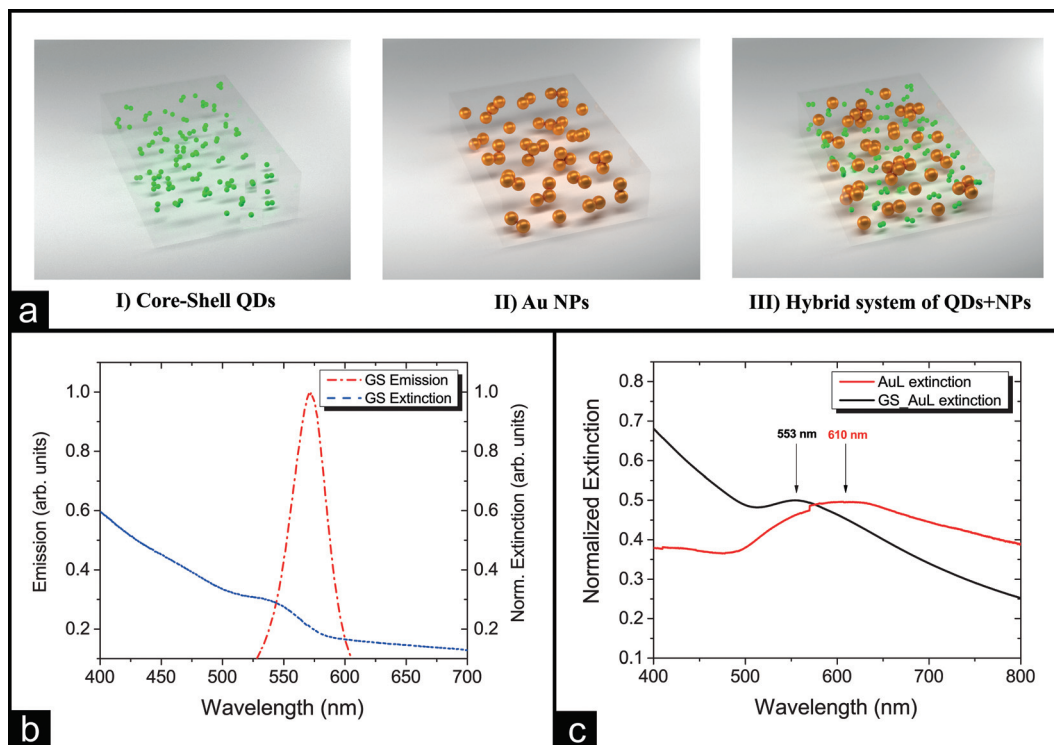


**Fig. 1** (a) A schematic of fabricated nanocomposite PDMS films with embedded (I) CdSe@ZnS QDs (GS), (II) Au NPs (AuL, AuH) and (III) mixture of Au NPs and QDs (GS\_AuL, GS\_AuH). (b) The QDs' normalized extinction and emission. The emission maximum is  $\approx 570$  nm and extinction maximum is  $\approx 545$  nm. (c) The extinction spectrum of AuL and GS\_AuL. AuL has a broad extinction due to NP aggregation. GS\_AuL extinction maximum is a convolution of the extinction of both QDs and NPs. An estimate of the "true" plasmon extinction of NPs is presented in ESI section 1† and its maximum is  $\approx 590$  nm.

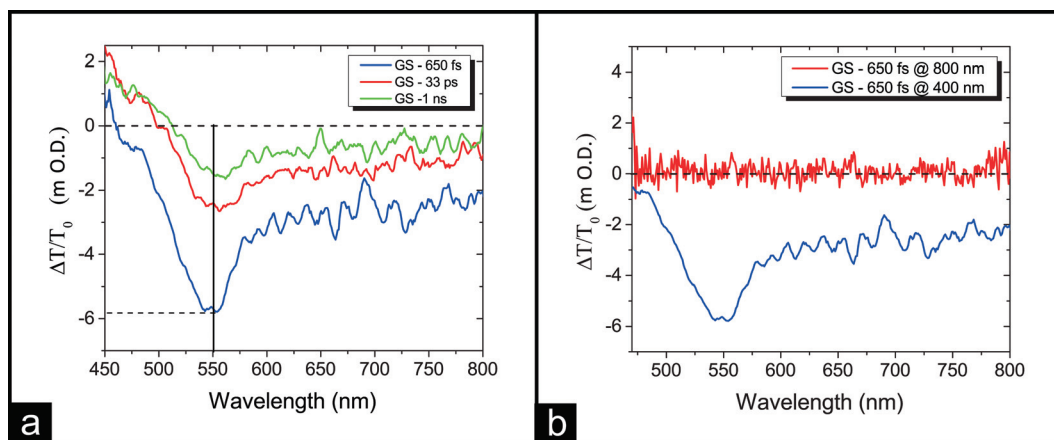


**Fig. 2** (a) Transient absorption (TA) results for GS for three delay times: 650 fs, 33 ps, and 1 ns for  $1 \mu\text{J}$  pump energy. We observe a broadband bleach that has a maximum around 550 nm due to the band filling effect. (b) Pumping GS with an 800 nm pump wavelength we observe no bleach since we are not exciting any QDs.

QDs' bleach in GS is mainly due to the well-known band filling effect<sup>21,22</sup> where the pump beam excites the valence band electrons to the conduction band. The TA signal for the band filling effect corresponds to a bleach effect reflecting the inability of exciting more electrons to the already populated states in the conduction band. On the other hand, exciting the

system with 800 nm does not cause any bleach as it is outside the QDs' absorption band (Fig. 2(b)).

Fig. 3(a) shows the TA spectrum of AuL at 650 fs, 1.3 ps and 2.5 ps delay times for 400 nm excitation pump wavelength and  $1 \mu\text{J}$  energy. The signal vanishes within the noise at around 3 ps. The bleach maximum wavelength is  $\approx 575$  nm, which

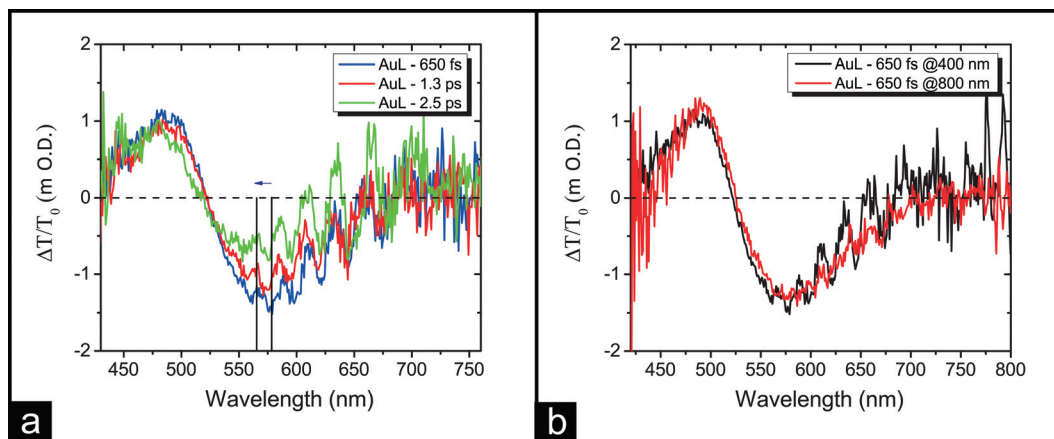


**Fig. 3** (a) TA results for AuL for three delay times: 650 fs, 1.3 ps, and 2.5 ps. The bleach maximum is  $\approx 575$  nm. The TA profile is due to the creation of hot electrons that modify the NPs' permittivity. An absorption wing appears at higher energies with respect to the bleach. There is another low energy absorption wing that is below the noise level. Additionally, the bleach maximum blue shifts as the delay time increases due to reduced EOPRD. (b) Excitation of AuL with 400 nm and 800 nm pump wavelengths after a 650 fs probe delay exhibits similar TA behavior.

blue shifts over time. Additionally, we observe a positive absorption band at the higher energy side of the bleach.

Generally, the excitation of mono-dispersed Au NPs results in plasmon bleaching feature; *i.e.* transient quenching and broadening of the plasmon band.<sup>23</sup> Accordingly, the  $(\Delta T/T_0)$  figure features a transient bleach centered at the plasmon band absorption maximum and two positive absorption bands (or wings) at lower and higher energies relative to the bleach. This is attributed to modifying the NPs' permittivity due to the creation of hot electrons, *i.e.* electrons that thermalize after absorbing the EM field energy due to a scattering event and are at an elevated temperature with respect to the metal lattice.<sup>24</sup> Upon pumping the NPs, the plasmon band broadens spectrally and its maximum peak intensity drops, *i.e.* the plasmon resonance quality factor decreases. This drop in the plasmon resonance quality factor indicates the existence of an extra damping or loss mechanism of the oscillating free electrons as we have discussed earlier. Hot electrons are more likely to experience scattering according to the Fermi liquid theory.<sup>24,25</sup> Furthermore, hot electrons have an augmented velocity due to their thermalization which makes them more amenable to surface scattering as well as collision-less Landau damping that occurs for the plasma oscillation of hot electrons.<sup>26</sup> It is important to emphasize that the quality factor of the plasmon resonance is not a steady state property. In practice, exciting the NP directly or indirectly, *e.g.* by exciting the gain, introduces additional losses and thus modifies the plasmon resonance transient quality factor.

Previous works have shown that the transient absorption bands/wings of pumped NP aggregates are uneven.<sup>27,28</sup> The higher energy absorption wing is larger in magnitude than the lower energy wing. We also observe two uneven transient absorption wings; however, the lower energy wing magnitude is lower than the noise level as we prove in ESI section 3.† Fig. 3(a) shows a blue-shift in the bleach maxima as a function of the delay time for AuL. This is due to the faster transient

bleach decay for longer wavelengths compared to shorter wavelengths. The blue shift of the bleach peak for NP aggregates is attributed to a reduction in the EOPRD.<sup>28</sup> EOPRD reflects the coupling strength between the electron oscillation frequency and the phonon modes of a given NP such that the smaller the detuning the stronger the coupling. The electron oscillation frequency is equal to  $v_f/R$  where  $v_f$  is the Fermi velocity and  $R$  is the domain radius. For very small domains, the electron oscillation frequency exceeds the Debye frequency of phonons which corresponds to the upper bound of the phonon mode spectrum. This frequency detuning decreases the electron-phonon coupling strength.<sup>29</sup> Given that hot electrons cool down by exciting phonons *via* electron-phonon scattering, the smaller the frequency detuning, the stronger the electron-phonon coupling and the faster the decay of the transient absorption/bleach. It has been suggested previously<sup>28</sup> that the probe beam interrogates a particular subset of the aggregates that corresponds to the excited resonance. For NP aggregates, resonances that correspond to longer wavelengths have larger domain radii which enhance the coupling to phonon modes.<sup>30</sup> Accordingly, longer wavelengths should experience faster decay kinetics of the TA spectrum compared to shorter ones resulting in the observed blue shift in the bleach maxima as a function of delay time. This is not the case for mono-dispersed NPs, where increasing the NP size decreases EOPRD, but also decreases the electron-surface scattering rate resulting in seemingly size independent decay kinetics.<sup>29,31</sup> It is important to note that exciting AuL at 800 nm (see Fig. 3(b)) results in a similar bleach as that of 400 nm excitation.<sup>31</sup>

For the hybrid system (GS\_AuL), we have shown previously that the gain is coupled *via* non-radiative energy transfer to the embedded plasmonic NPs *via* time resolved spectroscopy and pump-probe spectroscopy.<sup>32</sup> Here we are interested in the transient dynamics of loss mitigation in such a hybrid system. Fig. 4(a) shows the transient absorption results for GS\_AuL at 650 fs, 2.5 ps and 10 ps delay times for a 400 nm excitation pump wave-



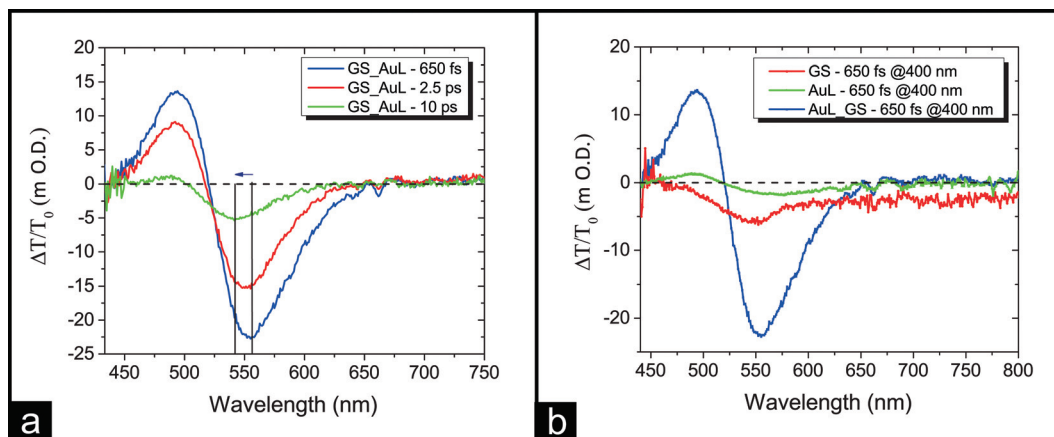


**Fig. 4** (a) TA results for **GS\_AuL** for 650 fs, 2.5 ps, and 10 ps delay times. The bleach maxima blue shifts as a function of the delay time due to reduced EOPRD. In (b) we compare the bleach magnitude for **GS**, **AuL** and **GS\_AuL**. The bleach is considerably stronger for **GS\_AuL** than the combined bleach of both **GS** and **AuL** indicating the existence of loss mitigation. However, the TA spectra of **AuL** and **GS\_AuL** are qualitatively similar.

length and 1  $\mu\text{J}$  energy. We observe a transient bleach band, and two uneven transient absorption wings. Compared to the TA results of both **GS** and **AuL**, the bleach signal of the hybrid system is considerably higher than the combined bleach of **GS** and **AuL** (see Fig. 4(b)). This observation quantitatively proves the existence of loss mitigation indicated by a significant enhancement in transmission. To further confirm our results, we performed UTAS measurements on **GS\_AuH** and obtained the same behavior of **GS\_AuL** (see section 3 in the ESI†).

From a qualitative point of view, however, **AuL** and **GS\_AuL** provide very similar TA spectra (Fig. 4(b)). This may be misinterpreted as loss mitigation and it is a consideration that was largely ignored by previous works.<sup>15</sup> In addition, performing a transient measurement by varying the delay time between the pump and probe beams cannot exclude such an effect because it is also a transient phenomenon. It is necessary to note that the modifications of NP permittivity due to the creation of hot electrons and due to loss mitigation are completely different phenomena. The plasmon bleaching of NPs due to the creation of hot electrons results in a simultaneous drop in absorption as well as scattering of the electromagnetic field by the NPs, *i.e.* the NP polarizability drops<sup>33</sup> and a new source of damping and loss is created. However, for the case of loss compensation, the final goal is to decrease the NP absorption while increasing its scattering<sup>11</sup> through providing energy to the quasi-static plasmon field in order to compensate for electron oscillation damping. On the other hand, the two effects produce a similar TA spectrum; both produce bleach within a certain spectral range, and an increase in absorption in a contingent spectral range. For the case of loss compensation, however, the absorption increase is a consequence of Kramers–Kronig integral relations<sup>14,15</sup> and not due to a drop in the resonance quality factor as in the case for NPs only in **AuL**.

One way to distinguish between these two effects is to perform transient reflection spectroscopy (TRS) in addition to TAS. If the bleach in TAS spectrally corresponds to a drop in

scattering in TRS, then this is merely due to modifying the NPs permittivity.<sup>13,33</sup> However, TRS is not a suitable technique for our system because embedding the NPs in a dielectric host reduces scattering significantly and thus results in a very low signal to noise ratio.

Another way to exclude the effect of pump induced permittivity modification is by pumping the hybrid system away from the gain absorption. Therefore, we pump **GS\_AuL** at 800 nm with a pump energy of 1  $\mu\text{J}$  (see Fig. 5). It is clear that the bleach for 800 nm excitation is significantly lower than that for 400 nm unlike what we have seen earlier in Fig. 3(b) for **AuL**. The same behavior of **GS\_AuL** was observed for **GS\_AuH** and is shown in Fig. S3 in ESI section 3.†

Fig. 4(a) shows that the bleach maxima also blue shifts over time. This blue shift is in part due to the decreased EOPRD of hot electrons in NP aggregates at longer wavelengths resulting from direct absorption of the excitation beam as we detailed previously for the case of the **AuL** system. However, induced bleach due to loss mitigation should also exhibit a similar blue shift. This is because electron–phonon scattering plays a dual role: (a) it mediates the absorption of electromagnetic energy creating hot electrons, and (b) it cools down hot electrons by transferring their extra heat to the lattice through phonons. In the case of loss mitigation, oscillating electrons at longer wavelengths in NP aggregates also experience stronger electron–phonon scattering because of their lower EOPRD. This means that enhanced transmission due to loss mitigation at longer wavelengths should decay faster than that at shorter wavelengths because of the existence of stronger damping, mediated by electron–phonon scattering. The enhanced electron–phonon scattering rate for longer wavelengths is of considerable significance. Although, it has been suggested that red-shifting the plasmon resonance of noble metals would allow them to exhibit lower losses,<sup>34</sup> this suggestion ignores the introduction of an extra transient loss mechanism, *i.e.* decreased EOPRD at longer wavelengths.

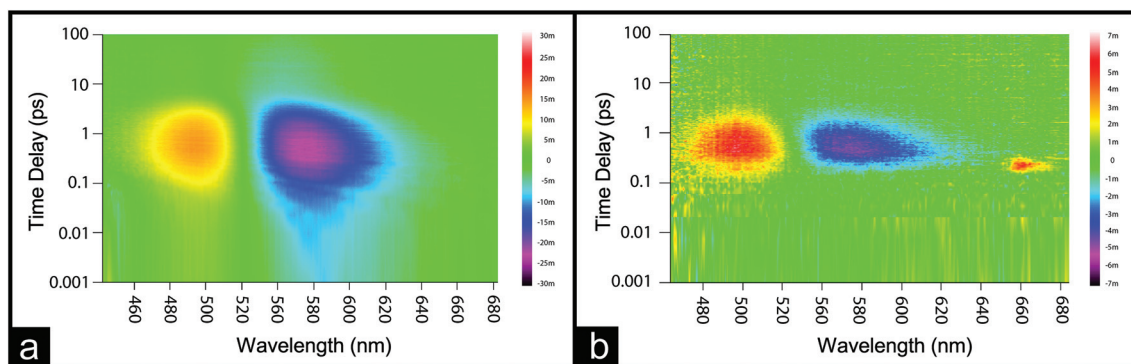


Fig. 5 Bird-eye view diagrams of GS\_AuL for pump wavelengths (a) 400 nm (b) 800 nm. The TA signal magnitude is considerably higher for the 400 nm excitation compared to the 800 nm excitation. At 800 nm we do not excite the gain and thus we exclude the contribution from loss compensation to the bleach.

While it has been shown previously that loss mitigation can be optimized for the case of Au core–gain shell aggregates due to enhanced field localization,<sup>35</sup> one should take into account the transient dynamics of such compensation. Compensating losses of the subset of SP resonances that experience stronger damping, in our case resonances at longer wavelengths due to EOPRD, decreases the efficiency of loss compensation over time.<sup>10</sup>

Furthermore, for 400 nm excitation the bleach maximum wavelength shifts as a function of pump power. As shown in Fig. 6, the maximum bleach wavelength starts at  $\approx 551$  nm for 0.5  $\mu\text{J}$  and progresses towards  $\approx 570$  nm which corresponds to the maximum emission wavelength. The maximum bleach wavelength was determined by using a polynomial fit to the bleach curve. This frequency pulling like effect of the bleach maximum is due to enhanced loss mitigation at the maximum emission wavelength as a function of pump energy. For AuL,

see ESI section 4,<sup>†</sup> we observe no shift in the bleach maximum as a function of pump energy. A similar behavior was reported theoretically in ref. 15. The authors defined the figure of merit (FOM) of loss mitigation as  $\text{FOM} = \text{Re}\{n\}/\text{Im}\{n\}$ . The FOM increased as a function of pump intensity and the maximum FOM wavelength shifted towards the maximum emission wavelength of the gain.<sup>15</sup> Since the probe beam interrogates the subset of aggregates that correspond to a given excited resonance, we can conclude that loss mitigation occurs for electromagnetically coupled NP aggregates for the subset of frequencies that correspond to the gain emission and depends on the loss mitigation efficiency at each emission wavelength.

### 2.3 Transient decay kinetics

The transient decay kinetics of exciton–plasmon resonant hybrids provides a panoramic view on the evolution of the loss mitigation process over time. In particular, it allows us to study the non-radiative exciton–plasmon energy transfer process by studying the decay kinetics of the transient absorption spectrum. Here we focus on the spectral region where the bleach occurs. The lifetimes are fitted by the following equation:

$$S(t) = e^{-\left(\frac{t-t_0}{\text{IRF}/2\ln 2}\right)^2} \times \sum_i A_i e^{-\frac{t-t_0}{\tau_i}} \quad (2)$$

where  $S(t)$  is the fitting function, IRF is the width of the instrument response function (full width at half maximum) and is set to be 0.1 ps corresponding to the pump pulse,  $t_0$  is time zero where the fitting starts,  $A_i$  and  $\tau_i$  are the amplitudes and decay times respectively.

The transient kinetics results of GS, AuL, AuH, GS\_AuL, and GS\_AuH at 570 nm are presented in Table 1. In all samples, the first time component  $\tau_1$  is assigned to the increase in the bleach (for 400 nm excitation wavelength with 1  $\mu\text{J}$  pump energy), while all other components correspond to the decay of the bleach over time. For GS, the bleach decay has three lifetime components. An infinite lifetime means that it is longer than the maximum delay achievable

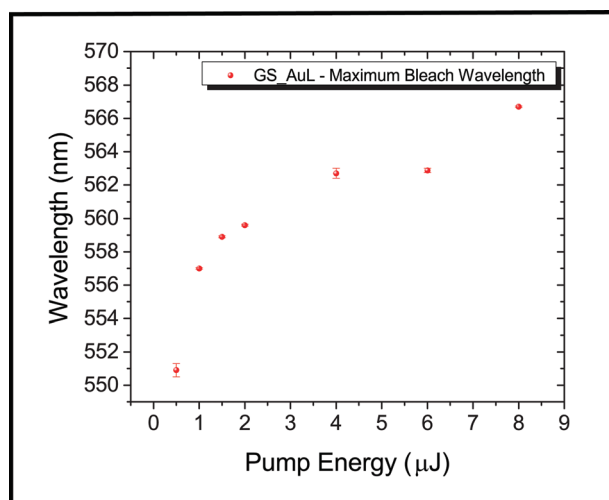
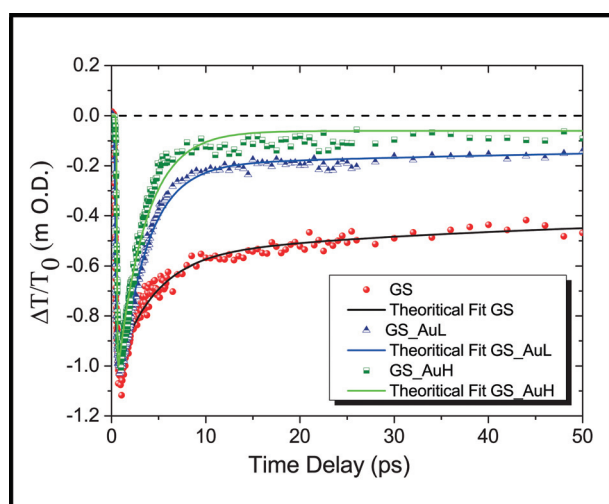


Fig. 6 Maximum bleach wavelength vs. pump energy for GS\_AuL. The maximum bleach wavelength shift is pulled towards the emission maximum of the coupled gain due to enhanced loss mitigation as a function of pump power.

**Table 1** The transient kinetics results of **GS**, **AuL**, **AuH**, **GS\_AuL** and **GS\_AuH**. Eqn (2) is used to fit lifetime results of all samples to extract the decay time components

Sample	$\tau_1$ (ps)	$\tau_2$ (ps)	$\tau_3$ (ps)	$\tau_4$ (ps)
<b>GS</b>	$0.15 \pm 0.02$	$3.1 \pm 0.3$	$737 \pm 150$	Inf.
<b>AuL</b>	$0.17 \pm 0.1$	$2.6 \pm 0.5$	Inf.	—
<b>AuH</b>	$0.17 \pm 0.07$	$1.8 \pm 0.2$	Inf.	—
<b>GS_AuL</b>	$0.19 \pm 0.01$	$2.45 \pm 0.09$	$115 \pm 32$	Inf.
<b>GS_AuH</b>	$0.2 \pm 0.06$	$2.1 \pm 0.2$	Inf.	—

by our setup. For **AuL** and **AuH** we have one bleach rise lifetime component ( $\tau_1$ ) and two bleach decay lifetime components ( $\tau_2$  and  $\tau_3$ ). The first lifetime component ( $\tau_1$ ) reflects electron–electron scattering that thermalizes the electron gas creating a Fermi distribution of hot electrons which results in the observed bleach. The bleach decay components ( $\tau_2$ ) and ( $\tau_3$ ) correspond to electron–phonon relaxation and phonon–phonon relaxation respectively.<sup>24</sup> Interestingly, the decay kinetics for **GS\_AuL** shows similar behavior to that of **GS** as they share the same lifetime components with shorter bleach decay lifetimes ( $\tau_2$  and  $\tau_3$ ) for **GS\_AuL** compared to **GS**. The decay kinetics of the hybrid system dynamics reflects both the drop in the bleach due to hot electron cooling as well as the decay in loss compensation efficiency over time as the (donor) gain depletes due to transferring its energy to the (acceptor) plasmonic NPs. When we have a high plasmonic NP concentration as in **GS\_AuH**, the gain depletion process becomes more efficient and the decay kinetics starts to look similar to that of a pure plasmonic system. Accordingly, the decay dynamics of the hybrid system has gain like and plasmon like features where the gain tends to increase the bleach lifetime and the energy transfer accompanied by plasmonic losses tends to decrease it (see Fig. 7).



**Fig. 7** Transient bleach dynamics results of **GS**, **GS\_AuL** and **GS\_AuH** and their theoretical fitting. The shortening of the bleach decay time for **GS\_AuH** compared to **GS\_AuL** reflects the effect of increasing the acceptor's concentration on gain depletion.

The observed behavior of the decay kinetics highlights the fact that gain mediated loss mitigation is a transient phenomenon by its nature as the gain itself depletes over time. It also shows that gain mediated loss mitigation does not eliminate losses like other strategies.<sup>8</sup> Oscillating electrons will still scatter and the energy will be absorbed with or without the gain. The existence of the gain, however, maintains the resonant response of oscillating free electrons from decaying by transferring energy over time to the quasi-static field of the plasmonic nanoparticles.

### 3 Conclusion

In summary, we have studied the ultrafast dynamics of coupled core–shell CdSe@ZnS QDs, and Au NP aggregates *via* femtosecond TAS. By studying the TA signal of QDs only and Au NPs only, we were able to separate loss mitigation in hybrid exciton–plasmon nano-assemblies from other effects that also enhance the transient transmission (bleach). Additionally, we showed a frequency pulling like effect of the transient bleach signal towards the emission maximum of the gain; an effect that has been previously predicted theoretically.<sup>15</sup> Furthermore, we presented that loss mitigation can occur for the subset of resonances of NP aggregates that overlap with the gain emission. Finally, we have investigated the transient kinetics of the bleach for all systems. The hybrid gain–plasmon systems have hybrid bleach decay dynamics reflecting the non-radiative energy transfer process between the gain (donor) and plasmonic NPs (acceptor).

This work provides a deeper understanding of exciton–plasmon dynamics to control optical losses in plasmonic nanostructures. Exciting the NPs directly creates hot electrons which suffer from more losses compared to cold electrons. To reduce optical losses, it is important to minimize the excitation of hot electrons. The excitation of hot electrons can be moderated by increasing the gain concentration in the presence of plasmonic NP aggregates since most of the pump energy will be absorbed by the gain, as proven by our TAS analysis. Furthermore, we reported that by increasing EOPRD we have decreased electron–phonon coupling, and this increases the loss mitigation efficiency. While other works<sup>36</sup> attempted to directly improve the quality factor of plasmon resonance through a careful choice of materials and design of plasmonic nanostructures, performing TAS analysis opens a new venue for investigating and optimizing the transient quality factor of plasmon resonance and eventually controlling losses in selected frequency ranges.

### 4 Experimental

#### 4.1 Preparation of nanocomposite hybrid systems

The elastomer was mixed thoroughly with the curing agent in the weight ratio of 10 : 1 and then degassed under vacuum to remove entrapped air bubbles. Au NPs (100  $\mu\text{L}$ ,  $3 \times 10^{-6}$  M

solution in hexane) and/or QDs (100  $\mu\text{L}$ ,  $6 \times 10^{-5}$  M solution in hexane) were added to the pre-polymer mixture (2 g) and vigorously stirred for 1 h to obtain a homogeneous mixture. The resulting mixtures were cast into a support template (2.5 cm  $\times$  2.5 cm) and the films were cured at 70  $^{\circ}\text{C}$  for 24 h to obtain *ca.* 3 mm thick self-standing films. The detailed information about the synthesis procedure of QDs and Au NPs can be found in ref. 37.

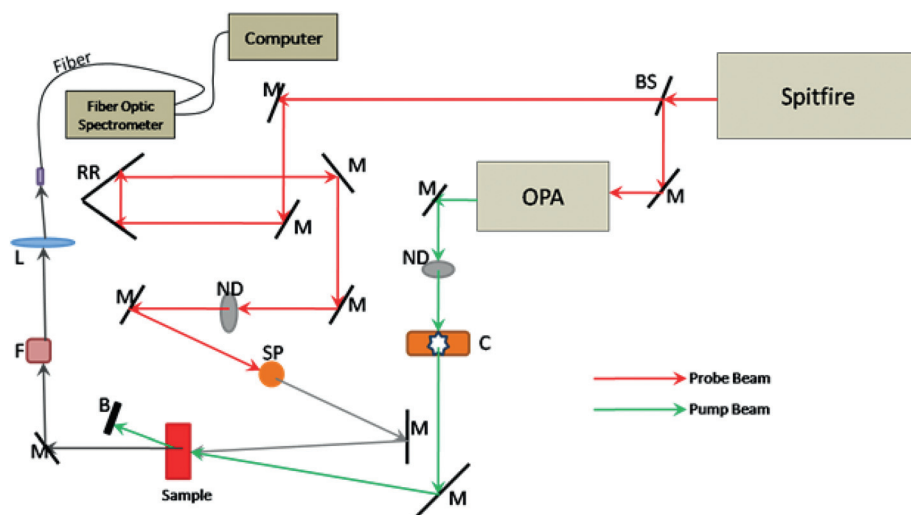
## 4.2 Characterization and measurements

The extinction was measured using a Cary 300 UV-VIS spectrophotometer, whereas the steady-state emission spectra were measured by means of an advanced fluorescence lifetime spectrometer (Edinburgh, FLS980 Series), equipped with a CCD camera (Andor, iDus 420 Series), a 450 W xenon arc lamp, high performance triple grating monochromators with integrated filter wheels, and a Hamamatsu MCP-PMT.

Ultrafast transient absorption spectroscopy experiments were carried out on all samples using a Ti:sapphire laser amplifier-optical parametric amplifier system (Spectra Physics) with 44 fs pulse duration and a 1 kHz repetition rate. A commercial pump-probe experimental setup with a white light continuum probe beam (Spectra Physics) was used (for more details see Scheme 1). Experiments were performed in the transmission geometry. The pulse duration is 100 fs inside the pump-probe experimental setup. The sample is pumped with a tunable output of the optical parametric amplifier. The excitation wavelength of the pump beam is set based on the energy levels of the target sample. The OPA unit provides the possibility to vary the output wavelength of the pump beam at a wide spectral range of 250 nm to 2800 nm. A white light continuum used as the probe beam is generated by impinging the 800 nm wavelength light of the Spitfire unit on a sapphire plate. This broadband beam (350 nm–800 nm) is used to

monitor the occurred transitions of the electrons to the allowed energy levels of the sample. Repetition rates of the pump and probe beams are 500 Hz and 1 kHz respectively. As a result of this matter, the effect of the pump beam will be observed only in one of the two consecutive probe beams. Both the pump and probe beams should overlap spatially and temporally over the sample. However, transmitted probe spectra are detected with a fiber optic spectrometer while the pump beam is dumped.

In the pump-probe technique, the ground state electrons are transferred to the excited states by applying a proper wavelength and energy values of the pump beam. A neutral density filter is used to modify the pump beam power. Consecutive probe spectra with lower intensity are used to extract the changes in spectra due to the pump pulses. The promoted electrons by the pump beam to the first excited state can be transferred to the higher permitted energy levels by the probe beam. Therefore, in the absence of the pump beam, the probe beam can cause the linear absorption, while in simultaneous presence of pump and probe beams, both linear and non-linear absorptions can occur. In order to measure the time duration for which electrons remain in different energy levels, the probe beams must be delayed against the pump beam. Such a delay is applied by using a motorized retro-reflector mirror in the path of the probe beam. The maximum delay of 3 ns between the pump and probe pulses can be created by the retro-reflector mirror. The zero reference time is considered as the time that both temporally synchronized pump and probe pulses hit over the sample. Therefore, at the point of zero time, the majority of the firstly excited electrons will be promoted to the higher excited states. The successive probe pulses will be delayed increasingly with respect to the pump pulses, by traveling in longer beam paths created by the retro-reflector mirror. In this case, a portion of the primarily pro-



**Scheme 1** Schematic representation of the pump-probe spectroscopy setup. M: mirror, L: lens, BS: beam splitter, C: chopper B: beam blocker, F: filter, ND: natural density filter, RR: retro-reflector mirror, SP: sapphire plate, OPA: optical parametric amplifier.



moted electrons to the first excited state return to the ground state by the aid of the broadband probe beam. In the meantime, the number of electrons stimulated to the higher excited states by the probe light will decrease exponentially. As a result of the exponentially decaying behavior of the observed non-linear effects, at a specific wavelength of the white beam spectrum the decay time of the transient effects can be measured.

## Acknowledgements

The research leading to these results has received support and funding from the Ohio Third Frontier Project Research Cluster on Surfaces in Advanced Materials (RC-SAM) at Case Western Reserve University. This work was supported by Projects DPT-HAMIT and NATO-SET-193. One of the authors (E. O.) acknowledges partial support from the Turkish Academy of Sciences. H. C. acknowledges support from the Science Academy of Turkey through the BAGEP programme and Turkish Academy of Sciences through the GEBIP programme.

## References

- 1 H. A. Atwater, *Sci. Am.*, 2007, **296**, 56.
- 2 J. B. Pendry and D. R. Smith, *Sci. Am.*, 2006, **295**, 60.
- 3 E. Ozbay, *Science*, 2006, **311**, 189.
- 4 S. Schlücker, *Angew. Chem., Int. Ed.*, 2014, **53**, 4756.
- 5 X. Huang and M. A. El-Sayed, *J. Adv. Res.*, 2010, **1**, 13.
- 6 M. Hedayati and F. Faupel, *J. Materials*, 2014, **7**, 1996.
- 7 C. M. Watts, X. L. Liu and W. J. Padilla, *Adv. Mater.*, 2012, **24**, 98.
- 8 J. B. Khurgin, *Nat. Nanotechnol.*, 2015, **10**, 2.
- 9 U. Kreibig and C. V. Fragstein, *Phys.*, 1969, **224**, 307.
- 10 M. El Kabbash, R. A. Rashed, K. V. Sreekanth, A. De Luca, M. Infusino and G. Strangi, *J. Nanomater.*, 2016, **2016**, 1.
- 11 N. M. Lawandy, *Appl. Phys. Lett.*, 2004, **85**, 5040.
- 12 G. Strangi, A. De Luca, S. Ravaine, M. Ferrie and R. Bartolino, *Appl. Phys. Lett.*, 2011, **98**, 251912.
- 13 A. De Luca, M. P. Grzelczak, I. Pastoriza-Santos, L. M. Liz-Marzan, M. La Deda, M. Striccoli and G. Strangi, *ACS Nano*, 2011, **5**, 5823.
- 14 M. Infusino, A. De Luca, A. Veltri, C. Vazquez-Vazquez, M. A. Correa-Duarte, R. Dhama and G. Strangi, *ACS Photonics*, 2014, **1**, 371.
- 15 S. Xiao, V. P. Drachev, A. V. Kildishev, X. Ni, U. K. Chettiar, H.-K. Yuan and V. M. Shalaev, *Nature*, 2010, **466**, 735.
- 16 O. Hess, J. B. Pendry, S. A. Maier, R. F. Oulton and J. M. Hamm, *Nat. Mater.*, 2012, **11**, 573.
- 17 N. Meinzer, M. Ruther, S. Linden, C. M. Soukoulis, G. Khitrova, J. Hendrickson, J. D. Olitzky, H. M. Gibbs and M. Wegener, *Opt. Express*, 2010, **18**, 24140.
- 18 J. Y. Suh, C. H. Kim, W. Zhou, M. D. Huntington, T. D. Co, M. R. Wasielewski and T. W. Odom, *Nano Lett.*, 2012, **12**, 5769.
- 19 J. M. Hamm, S. Wuestner, K. L. Tsakmakidis and O. Hess, *Phys. Rev. Lett.*, 2011, **107**, 167405.
- 20 M. Quinten and U. Kreibig, *Surf. Sci.*, 1986, **172**, 557.
- 21 C. Burda, S. Link, T. C. Green and M. A. El-Sayed, *J. Phys. Chem. B*, 1999, **103**, 10775.
- 22 S. Hunsche, T. Dekorsy, V. Klimov and H. Kurz, *Appl. Phys. B*, 1996, **62**, 3.
- 23 X. Wang, Y. Guillet, P. R. Selvakannan, H. Remita and B. Palpant, *J. Phys. Chem. B*, 2015, **119**, 7416.
- 24 S. Link and M. A. El-Sayed, *J. Phys. Chem. B*, 1999, **103**, 8410.
- 25 T. S. Ahmadi, S. L. Logunov and M. A. El-Sayed, *J. Phys. Chem. B*, 1999, **100**, 8059.
- 26 D. D. Ryutov, *Plasma Phys. Controlled Fusion*, 1999, **41**, A1.
- 27 P. K. Jain, W. Qian and M. A. El-Sayed, *J. Phys. Chem. B*, 2006, **110**, 136.
- 28 C. D. Grant, A. M. Schwartzberg, T. J. Norman and J. Z. Zhang, *J. Am. Chem. Soc.*, 2003, **125**, 549.
- 29 M. J. Feldstein, C. D. Keating, Y. H. Liau, M. J. Natan and N. F. Scherer, *J. Am. Chem. Soc.*, 1997, **119**, 6638.
- 30 B. A. Smith, J. Z. Zhang, U. Giebel and G. Schmid, *Chem. Phys. Lett.*, 1997, **270**, 139.
- 31 S. Link and M. A. El-Sayed, *Int. Rev. Phys. Chem.*, 2000, **19**(3), 409.
- 32 R. Dhama, A. R. Rashed, V. Caligiuri, M. El Kabbash, G. Strangi and A. De Luca, *Opt. Express*, 2016, **24**(13), 14632.
- 33 R. W. Schoenlein, W. Z. Lin, J. G. Fujimoto and G. L. Esley, *Phys. Rev. Lett.*, 1987, **58**, 1680.
- 34 R. F. Oulton, *Nat. Photonics*, 2012, **6**, 219.
- 35 A. R. Rashed, A. De Luca, R. Dhama, A. Hosseinzadeh, M. Infusino, M. El Kabbash, S. Ravaine, R. Bartolino and G. Strangi, *RSC Adv.*, 2015, **5**, 53245.
- 36 G. Lilley, M. Messner and K. Unterrainer, *Opt. Mater. Express*, 2015, **5**, 2112.
- 37 A. De Luca, N. Depalo, N. E. Fanizza, M. Striccoli, M. L. Curri, M. Infusino, A. R. Rashed, M. La Deda and G. Strangi, *Nanoscale*, 2013, **5**, 6097.